DEUTSCHES ELEKTRONEN-SYNCHROTRON DESY

DESY SR 84-32
November 1984

SHAPE RESONANCES AND PARTIAL PHOTOEMISSION CROSS SECTIONS OF SOLID SF_6 AND CCl_4

by

J.-H. Fock

II. Institut f. Experimentalphysik, Universität Hamburg

E.E. Koch

Hamburger Synchrotronstrahlungslabor HASYLAB at DESY, Hamburg

ISSN 0723-7979

NOTKESTRASSE 85 · 2 HAMBURG 52

To be sure that your preprints are promptly included in the
HIGH ENERGY PHYSICS INDEX ,
send them to the following address (if possible by air mail) :

DESY
Bibliothek
Notkestrasse 85
2 Hamburg 52
Germany

DESY SR 84-32
November 1984

ISSN 0723-7979

Shape resonances and partial photoemission cross sections of solid SF_6 and CCl_4 *

J.-H. Fock#
II. Institut für Experimentalphysik, Universität Hamburg,
D-2000 Hamburg 50, Fed. Rep. Germany

and

E.E. Koch
Hamburger Synchrotronstrahlungslabor HASYLAB at DESY
D-2000 Hamburg 52, Fed. Rep. Germany

Abstract

Photoelectron energy distribution curves from solid films of SF_6 and CCl_4 have been measured in the photon energy range 10 eV $\leq h\nu \leq$ 40 eV using synchrotron radiation. The binding energies, peak-widths and relative partial cross sections have been determined. In the photoelectron spectra a 1:1 correspondence to the gasphase is observed for the occupied molecular orbitals, and a straight forward assignment of the occupied valence bands emerges. Furthermore, the cross sections of the individual orbitals show for both samples great similarities to the gas phase. For SF_6 detailed structures are visible in the cross sections which are only partly interpreted as shape resonances. A new assignment for the $6t_{1u}$ shape resonance is proposed and the resonance energies are related to X-ray absorption and electron scattering data. Furthermore a comparison of the total photoemission cross section to the optical reflection spectrum of solid SF_6 is presented. For CCl_4 less structures are observed in the partial cross sections. They are all interpreted as shape resonances. An energetic scheme of the virtual orbitals is proposed for CCl_4.

* Work supported in part by Bundesministerium für Forschung und Technologie (BMFT) from funds for research with synchrotron radiation

now at: Valvo-RHW, Stresemannallee 101, D-2000 Hamburg 54, Fed. Rep. Germany

submitted to Chem. Phys.

Introduction

Partial photoionisation cross sections and shape resonances are now widely studied for a growing number of molecules. They play a major role in photoabsorption from core levels, in molecular photoionization and in electron scattering. Experimental investigations for gaseous molecules, molecules adsorbed on surfaces and solid molecular films have been accompanied by intense theoretical efforts to understand and quantitatively describe the cross sections and resonances. These combined efforts have provided detailed information concerning the energetics and dynamics of final states [1-17].

Molecular shape resonances have been discussed under various aspects. For our following considerations we define it here as a single particle quasibound state which is trapped by a potential barrier. The potential barrier concept has at least two origins: (i) the so called "inner well" states associated with a two valley potential, which were used for the interpretation of absorption spectra at the K- and L-edges of cagelike molecules such as SF_6 [1,2] and (ii) the temporarily negative ion resonance states trapped in a centrifugal barrier as observed and discussed in electron scattering experiments [14,17]. As became apparent later both concepts have much in common and can be described by a multiple scattering approach or within the Hartree-Fock approximation including unoccupied virtual valence orbitals.

For a qualitative discussion of shape resonances we refer to Fig. 1 [18]. The effective potential barrier surrounding the central atoms of the molecule devides the potential into an inner part and a shallow potential region at the periphery of the molecule. This concept of the double well potential was originally used for the discussion of the peculiarities in the SF_6 K- and L-edge absorption spectrum [1,2]. The absorption spectra show up to four distinct peaks, but almost no Rydberg series and no steplike structure at the inner shell thresholds was observed [2,19]. The potential barrier was considered to arise mainly from the electronegative fluorine atoms. While this intuitive static picture is still a good starting point for a qualitative discussion we emphasize that in small molecules the potential barrier is entirely formed by high angular momentum final state waves. For an angular momentum $l \geq 1$ the potential is given by an effective potential V_{eff} which is a superposition of an attractive Coulomb potential and a repulsive centrifugal barrier $V_{eff} \propto V_{Coul}(r) + l(l+1)/r^2$. Close to threshold shape resonances dominate the absorption and photoemission spectra of both

inner and outer shells as well as the cross sections of electron scattering on neutral molecules. Many examples of molecules showing shape resonances are known today, however, most of them are simple di- and triatomic species and little information is available on other cagelike molecules like e.g. CCl_4.

In the course of a systematic study of the band structure and the photoemission cross sections of molecular crystals [20-22] we present in this paper the first results for solid SF_6 and CCl_4. For both materials the cross sections as a function of photon energy show structures which can be related to shape resonances. In case of SF_6 the molecular origin of the resonances is discussed and related to X-ray absorption spectra, electron scattering data and to theoretical cross-section calculations. The energies of the resonances observed in different types of experiments can be arranged in a regular scheme, similar to our previous observations for solid N_2 and CO_2 [20,21], and comparison is made to the optical reflection spectrum. The CCl_4 data are discussed in terms of recent multiple scattering calculations [23] and preliminary gas phase results [24,25].

Experimental details

The experimental set-up used for our experiments has been described in detail elsewhere [21]. Here we give only a brief description: Synchrotron radiation from the DORIS II storage ring was monochromatized by a 3 m normal incidence monochromator at the HASYLAB laboratory in Hamburg. The photon energy range covered was between 10 eV and 40 eV. Electron energies were measured with an angle integrating double pass cylindrical mirror analyzer (CMA) operated in the retarding mode with a constant resolution (ΔE = 0.2 eV for $h\nu < 25$ eV ; ΔE = 0.4 for $h\nu \leq 30$ eV ; ΔE = 0.6 for $h\nu < 35$ eV and ΔE = 0.7 for $h\nu < 40$ eV). The total resolution was basically determined by the analyzer.

At low photon energies the resolution was sufficient to determine accurately the width of the observed structures in the electron distribution curves (EDS's) which ranged between 0.7 eV and 1.3 eV (FWHM).

Research grade SF_6 and CCl_4 were condensed onto the cold tip of a helium flow cryostat under UHV conditions ($p \approx 5 \times 10^{-10}$) at low temperatures. Freshly in situ evaporated films of gold (SF_6) or silver (CCl_4) were used as substrates. The evaporation of CCl_4 onto a freshly prepared silver substrate resulted in a surface reaction, where CCl_4 was decomposed into Cl chemisorbed

to Ag. This was obvious when we compared our measured EDCs with gas phase literature data [26,27]. The chemisorption increased the work function of the substrate by about 1.7 eV. For all subsequently prepared samples no further reaction was observed, so that pure polycrystalline molecular crystals of CCl_4 were formed. In the case of SF_6 on gold no reaction was observed.

During evaporation the whole chamber was exposed to the sample gas. This is different from our previous technique [20,21] where a capillary was used. Sample thicknesses were measured in Langmuir (1 Langmuir = 1 L = 10^{-6} torr sec; uncorrected ionization gauge reading) and were restricted to 55 L for SF_6 and 150 L for CCl_4 to avoid charging of the samples. The temperature of the substrate was as high as possible (T = 40 K for SF_6 and T = 70 K for CCl_4) during condensation to favour the growth of larger polycrystals. The EDC's were then measured with sample temperature below 20 K. Whenever charging was observed, a completely new sample was prepared.

Photoemission intensities were determined from the measured EDCs. Firstly all EDCs were normalized to the incoming photon flux. Secondly a smooth background of scattered electrons was subtracted from the spectra. Thirdly the observed peaks were fitted by gaussians in order to determine the peak areas. These areas are plotted as a function of photon energy to give the relative partial cross sections of the individual orbitals. Branching ratios were also determined and are also plotted as a function of photon energy.

As discussed elsewhere [21,28] neither the transmission function of the analyser nor the electron mean free path influence strongly the observed features in the cross section curves, so that our results may be directly compared to gas phase cross section data.

Results for solid SF_6

Sulphur hexafluoride is a molecule of octahedral symmetry (point group O_h) with a total of 70 electrons, of which 36 belong to the valence shell with binding energies below 30 eV. In fig. 2 the molecular orbital (MO) scheme is shown [29]. Although a great number of experimental and theoretical work has been published on the relative ordering of the valence levels no complete agreement could be reached between different authors. This problem has only recently been discussed again by Dehmer et al. [30], including a review

of the literature. We will follow their recommendation and utilize the electron configuration as given in fig. 2.

In fig. 3 the comparison of a gas and solid phase electron energy distribution curve is shown, which exhibits a one to one correspondence of the occupied valence levels which is already familiar from other molecular solids [20-22,31,32]. The origin of the additional peak in the solid spectrum at around 28 eV binding energy (kinetic energy E_{kin} = 12 eV) is not clear. It is either not present at lower photon energies or does not shift as the photon energy is lowered (see fig. 4). Most probably this peak is due to a second order process which must be stronger in the solid than in the gas phase[1)].

EDC's for solid SF_6 have not been measured before. In table 1 the observed binding energies (vertical and adiabatic) and widths of the peaks are collected and compared to the gas phase. In this table the MO-assignment is also given. We note that the bands are broadened in the solid phase and shifted towards lower binding energies. This broadening and relaxation shift is a general phenomenon for ionization potentials in monomolecular crystals which we have discussed in detail for the case of solid CO_2. Since we are mainly interested in the partial photoemission cross sections we do not repeat the discussion here but refer to our previous paper and references therein [21].

It is interesting to point out that the gas- and solid spectra in fig. 3 not only show the same valence orbitals in both phases but also the same relative intensities. The elucidation of the intensity variation of the individual orbitals with photon energy is the major aim of the present work. Therefore EDCs have been measured covering the range of photon energies from the onset of photoemission $h\nu$ = 15 eV to $h\nu$ = 40 eV as shown in fig. 4. After normalizing the incident photon flux and unfolding with gaussians as described in the experimental section, the intensities of individual peaks are plotted as a function of photon energy in figs. 5 and 6. All intensities are on the same relative scale. The scattering of data points can be considered as a rough estimate for the error. The solid lines are hand-

1) It seems that similar weak structures are present at kinetic energies E_{kin} = 3-4 eV in the photon energy range $h\nu$ = 22-28 eV and at E_{kin} = 8-9 eV in the range $h\nu$ = 28-32 eV.

drawn to guide the eye. For convenience the branching ratios are also given in fig. 7. In this case the scattering of data points is much less, as expected. The numerical values to figs. 5 - 7 are collected in the appendix.

The intensities shown in figs. 5 and 6 may be directly compared to gas phase cross section data, which have been measured by Gustafsson [33] and by Dehmer et al. [30]. In the overlapping region both sets of gas phase data agree well with each other.

Previously we have shown for data on solid N_2 [20] and solid CO_2 [21], that the cross sections of the solid phases were importantly different from the gas phase results. The differences were explained as arising from band structure effects in the solid. For solid C_2H_2 [22] on the other hand a very similar behaviour of gas phase and solid cross sections was observed, the main structure being due to autoionisation in this case. SF_6 is another example where the cross sections of the solid phase are largely identical to the gas phase. We would like to briefly comment on the partial cross sections of the individual valence orbitals. The energies of the observed structures in the partial cross sections are summarized in table 2. In the next section we discuss these findings in more detail.

$1t_{1g}$-orbital: The partial cross section for this orbital shows relatively rich structure with a total of five maxima (see fig. 5 and table 2) of which only the $h\nu$ = 27 eV feature is not visible in the gas phase.

$5t_{1u}$ + $1t_{2u}$-orbitals: Fig. 5 shows three maxima of which the first two are very strong. These two maxima are also present in the gas phase, although not so broad and therefore more clearly separated. The third peak at $h\nu$ = 29 eV is clearly seen in our spectra, however, the gas phase data of Gustafsson [33] show only a broad steplike structure in this energy region.

$3e_g$-orbital: This orbital shows a broad maximum at $h\nu$ = 22.5 eV and a second smaller one at $h\nu$ = 26.5 eV which is not seen in the gas phase data. The comparison with the gas phase cross section suggests that the first maximum consists of two peaks at $h\nu$ = 20 eV and $h\nu$ = 22.5 eV which are broadened and not separated in the solid phase.

$1t_{2g}$-orbital: Fig. 6 shows two peaks in the cross section, whereas in the gas phase only a very brod maximum is observed at the same energy.

$4t_{1u}$-orbital: The cross sections for gas and solid phase are practically identical showing a small peak at $h\nu$ = 23.5 eV and a big one at $h\nu$ = 28 eV, although in the solid the second peak is somewhat asymmetric with a shoulder at $h\nu$ = 30 eV.

$5a_{1g}$-orbital: No cross sections could be determined for this orbital close to threshold because of the secondary electron tail. Between $h\nu$ = 37 eV and 40 eV the intensity is small (see fig. 6).

In summary we found that all the observed structures in the gas phase partial cross sections of SF_6 are also present in the solid. Some of the observed deviations might be attributed to the fact that in the EDCs of the solid phase the individual peaks overlap, so that an unfolding procedure was necessary. However, we note that an additional peak in the cross sections of all gerade orbitals ($1t_{1g}$, $3e_g$, $1t_{2g}$) is observed at around $h\nu$ = 27 eV in the solid state.

Discussion for solid SF_6

SF_6 can be regarded as one of the nicest examples for the similar influence that shape resonances have on spectra measured with different experimental techniques. This becomes evident when absorption data, photoemission cross sections and electron scattering data are compared.

In the X-ray absorption spectra of the sulphur K- and L-shell and the fluorine K-shell four shape resonances, namely $6a_{1g}$, $6t_{1u}$, $2t_{2g}$ and $4e_g$, are observed. The first two resonances are below threshold and thus form discrete shape resonances, whereas the last two lie in the continuum. These four shape resonances correspond to the four lowest unoccupied valence orbitals of the molecule (see fig. 2).

As has been discussed by Dehmer and Dill [11,17], the same set of shape resonances which is observed in the absorption spectra of inner shells is also expected in the scattering cross sections of electrons on neutral molecules. In the latter case the shape resonances are shifted to higher kinetic energies due to stronger Coulombic repulsion. For SF_6 the electron scattering cross sections have been calculated by Dehmer et al. [34] and measured by Kennerly et al. [35]. Indeed all four shape resonances of SF_6 can be observed in electron scattering. In table 3 the energies are collected.

In the valence shell absorption and photoemission cross sections again the same four resonances should be visible. The kinetic energies are expected to lie between the inner shell absorption and electron scattering values, because of a different Coulombic interaction. For CO_2 [21] we were able to show that this expectation is true and a regular shift of the resonance energies occurs in going from inner shell absorption via the gas phase and solid phase valence shell absorption and photoemission to electron scattering on the neutral molecule. This regularity can be utilized in the interpretation of our cross section data. In fig. 8 the observed energies of the four shape resonances in x-ray absorption and electron scattering are plotted on a common energy scale and connected by straight lines. The figure shows, that for the valence shell absorption and photoemission the $6a_{1g}$ resonance should be expected below threshold. It would thus still be a discrete shape resonance, i.e. a valence transition which can not be observed in photoemission. The $6t_{1u}$ resonance should occur at threshold, whereas $2t_{2g}$ and $4e_g$ are expected at $E_{kin} \approx 6$ eV and 20 eV respectively well above threshold. Of course in our photoemission cross section data only the $2t_{2g}$ and $4e_g$ resonances above threshold should be visible.

The two gerade shape resonances $2t_{2g}$ and $4e_g$ can, according to dipole selection rules, only be reached from ungerade occupied valence orbitals, i.e. from $5t_{1u}$, $1t_{2u}$ and $4t_{1u}$. The $4t_{1u}$ cross section (Fig. 6) has a maximum at $h\nu$ = 28 eV which has already previously been assigned to the $4t_{1u} \rightarrow 2t_{2g}$ shape resonance [30,33,36]. The observed kinetic energy of E_{kin} = 6.1 eV fits rather well on the straight line in fig. 8.

As can be seen from fig. 5 a large maximum is observed at $h\nu$ = 23 eV or E_{kin} = 6.6 eV in the cross section curve of $1t_{2u} + 5t_{2u}$. It is again interpreted as the same shape resonance, namely $1t_{2u} \rightarrow 2t_{2g}$ and $5t_{1u} \rightarrow 2t_{2g}$ [30,31, 34]. Although one would expect the $4e_g$ shape resonance to occur in just the same cross sections, and calculations clearly predict this behaviour [30,36], no additional peak is visible in our spectra nor is it seen in gas phase data. The small peak at $h\nu$ = 29.0 eV in the $1t_{2u} + 5t_{1u}$ curve in fig. 5 is not likely to be due to this shape resonance, because the kinetic energy would be much too small. The reason why the $4e_g$ shape resonance is not observed in the valence shell is not clear yet. Averaging over vibrational levels might smear out the resonance. This effect has already been observed for other molecules [37].

A large number of other structures are visible in figs. 5 and 6. All gerade orbitals exhibit a maximum very close above threshold (see table 2), which we tentatively attribute to the $6t_{1u}$ shape resonance. As suggested by the linear plot in fig. 8 this resonance is expected right at threshold. The multiple scattering calculations of Wallace [38] place this resonance below threshold in the discrete part of the spectrum. We note, however, that the energies of resonances in this type of calculation can be off by several eV. Therefore this is no severe contradiction to our assignment.

For the remaining structures which we have not yet assigned it is obvious that simple one electron models are not sufficient to interprete them. Dehmer et al. [30] have proposed channel interaction and autoionization processes as possible mechanisms. Only recently we could show for solid acetylene [22] that autoionizing valence transitions can have a major influence on the cross sections of molecular crystals. That this is likely to be the case also for SF_6, is supported by the experimental observation that many of the observed structures in the cross sections of different orbitals are found at the same photon energy rather than at the same kinetic energy. For example all gerade orbitals ($1t_{1g}$, $3e_g$, $1t_{2g}$) show an unidentified maximum at $h\nu$ = 27 eV as already mentioned, which is not seen in the gas phase. This energy fits surprisingly well with an estimate Dehmer et al. [30] made for the valence transition or shape resonances $5a_{1g} \rightarrow 6t_{1u}$ at $h\nu \approx 26.7$ eV, which would be a plausible candidate for autoionization. This transition would occur directly at threshold in accordance with fig. 8.

Finally we would like to comment on our data from another point of view. From basic dielectric theory one can show that the imaginary part $\varepsilon_2(\omega)$ of the dielectric function should bear a close connection to the sum of the measured photoemission cross sections as we have already discussed in detail for the case of CO_2 [21]. Blechschmidt et al. [19] have measured the VUV reflection spectrum of solid SF_6. Due to the rather low reflectivity of solid SF_6 one can assume that the reflection is almost identical to $\varepsilon_2(\omega)$. This spectrum is reproduced in fig. 9 together with the sum of the photoemission cross sections which have been fitted to the reflection spectrum at $h\nu$ = 23 eV and 29 eV. The agreement is really good. It is thus possible to assign the maximum at $h\nu$ = 23 eV in the reflection spectrum on the basis of the results presented here as mainly arising from the $2t_{2g}$ shape resonance. Furthermore, the strong maximum at $h\nu$ = 16 eV in the reflection curve, which is not reproduced by the cross section curve, might well be related to the discrete $6a_{1g}$ shape resonance and thus be a Frenkel type exciton in solid state language.

Results and Discussion for solid CCl_4

CCl_4 is a molecule with certain structural similarities to SF_6. In both cases a central atom is surrounded by a cage of electronegative atoms. If it is true that these electronegative ligands are at least partly responsible for the occurrence and strength of shape resonances, CCl_4 is a good candiate to look for these effects in the partial photoemission cross sections. However, different from SF_6 which attracted a lot of attention over the last ten years, only a few studies have been done on CCl_4. Electron scattering experiments have not been performed to our knowledge and x-ray absorption experiments [39-42] have not been analysed in terms of shape resonances. Photoemission cross section data at high photon energies ($h\nu > 35$ eV) together with measurements of the asymmetry parameter β have been published [43] for the gas phase. In this energy region Cooper-Minima are observed which are typical for atomic 3p orbitals and molecular orbitals derived from them. At low energies ($h\nu < 30$ eV) only β-parameter measurements are available. The same group made available to us preliminary data of both experimental and theoretical [23-25] cross sections with which we can compare our measurements.

We start with a discussion of the molecular orbital scheme shown in fig. 10. The valence MO's of CCl_4 are formed by carbon 2s and 2p and chlorine 3p atomic orbitals. Among the first unoccupied MO's the chlorine 3d orbitals are expected to play a dominant role. The five uppermost occupied valence MO's $2t_1$ to $6a_1$ are clearly visible in the EDC's for solid CCl_4 as shown in fig. 11 at different photon energies. While the uppermost feature with highest kinetic energy is composed of three bands (see fig. 12) the $6t_2$ and $6a_1$ maxima are well separated. For high photon energies a maximum of scattered electrons around 2 eV kinetic energy is also visible. The direct emission features are decomposed into partly overlapping bands as indicated in fig. 12 for one particular photon energy. Thus a clear one to one correspondence to the gas-phase photoelectron spectrum of CCl_4 [44,45] emerges (fig. 12) and it is easy to assign the maxima for solid CCl_4 to the photoemission from valence bands formed by the $2t_1$, $7t_2$, 2e, $6t_2$, and $6a_1$ MO's of the CCl_4 molecule respectively. The resulting vertical and adiabatic binding energies are compiled in table 4 and compared to the gas phase values. From these data we obtain a rigid gas-to-solid shift (relaxation energy) towards lower binding energies of $\Delta E_R^{vert} = 1.33 \pm 0.1$ eV for all five emission bands. For a discussion of the relaxation energy as well as the solid state broadening effects we again refer to our previous paper and references therein [21].

The data reduction for obtaining the partial photoemission cross sections was done in exactly the same manner as already described for SF_6. From the family of EDCs measured at different photon energies shown in fig. 11 the relative partial cross sections and branching ratios were derived. They are shown in figs. 13 and 14 and corresponding numerical values are listed in the appendix.

A first glance at fig. 13 shows that the cross sections of CCl_4 are much less structured than was the case for SF_6. Although the first three uppermost orbitals $2t_1$, $7t_2$ and 2e are all of Cl 3p lone pair character (see fig. 10) they show a different behaviour at low photon energy. A similarity to atomic 3p cross sections when compared e.g. to Ar 3p is only obvious at higher photon energies where Cooper-Minima have been observed [43]. At low energies close to threshold molecular effects seem to play a major role.

In the following we discuss the individual orbitals. For convenience the allowed dipole transitions are listed in table 5. In table 6 the observed structures in the cross sections are summarized.

$2t_1$-orbital: The cross section of the $2t_1$ orbital shows two maxima (fig. 13). The gas phase results of Keller et al. [25] are practically identical to ours and show the same two maxima. According to table 5 four photoemission channels are open from $2t_1$. The multiple-scattering calculation of Grimm [23] finds negligible intensity in $2t_1 \rightarrow \varepsilon a_2$ whereas the other three channels are comparable in magnitude. $2t_1 \rightarrow \varepsilon t_2$ shows a smooth variation with photon energy, but both channels $2t_1 \rightarrow \varepsilon 1$ and $2t_1 \rightarrow \varepsilon a_2$ exhibit a shape resonance at the same kinetic energy $E_{kin} = 2.4$ eV [24]. Comparison of experiment and calculation makes it very probable that indeed two shape resonances are present, however, at different energies namely at $h\nu = 13.0$ eV ($E_{kin} = 2.7$ eV) and $h\nu = 15.5$ eV ($E_{kin} = 5.2$ eV). This deviation in energy leeds to only poor agreement between calculated and measured total cross sections.

$7t_2$-orbital: For the orbital $7t_2$ also two maxima are observed in the photoemission cross section at $h\nu = 13.5$ eV and $h\nu = 18.0$ eV and again two shape resonances are calculated to occur in the channels $7t_2 \rightarrow \varepsilon 1$ and $7t_2 \rightarrow \varepsilon t_2$. The other two allowed channels $7t_2 \rightarrow \varepsilon a_1$ and $7t_2 \rightarrow \varepsilon t_1$ have only very small intensity. The gas phase spectrum of Keller et al. [25] shows less pronounced maxima and a smaller intensity for this orbital. A possible reason for the difference might be that the unfolding procedure necessary for the solid state data leads to a systematic overestimation of the cross section for this band.

2e-orbital: The photoemission cross section of the third orbital 2e is again very similar in both the gas and the solid phase. Although the intensity is only weak, two broad maxima can be identified at $h\nu$ = 14.5 eV and $h\nu$ = 23.0 eV. The multiple scattering calculation predicts two shape resonances both in the $2e \rightarrow \varepsilon t_1$ channel. The second allowed channel $2e \rightarrow \varepsilon t_2$ has about the same intensity but does not show distinct resonances. The occurrence of two shape resonances in the same channel is very unusual and has not been observed before. On the other hand the molecular orbital scheme (fig. 10) shows many unoccupied orbitals among which two of t_1 symmetry can be found. Of course it is tempting to identify the two observed resonances with these virtual orbitals.

$6t_2$-orbital: The fourth orbital $6t_2$ is the first bonding one and should therefore behave different from the lone pair orbital $7t_2$ discussed above. Indeed our results show that this is the case. Only one broad maximum is observed at $h\nu$ = 18 eV. Gas phase measurements are not available but Grimm [23] has calcuated two shape resonances in the channel $6t_2 \rightarrow \varepsilon e$ and $6t_2 \rightarrow \varepsilon t_1$ which are quite far apart at $E_{kin} \approx 2.4$ eV and $E_{kin} = 8.4$ eV. The first one corresponds nicely with the observed maximum. As far as the second resonance is concerned, it is interesting to note that a small hump is observed in the branching ratio of the $6t_2$-orbital (fig. 14) at $h\nu$ = 25.0 eV (E_{kin} = 9.7 eV) which we tentatively assign as the calculated $6t_2 \rightarrow \varepsilon t_1$ shape resonance.

$6a_1$-orbital: The last valence orbital $6a_1$ measured in our experiments shows in agreement with Grimm's calculation only a small cross section. However, close to threshold it is not possible to distinguish the direct emission from this orbital unambigiously from the background of scattered electrons.

In summary we can say that the partial photoemission cross sections measured for the molecular crystal of CCl_4 are very similar to the gas phase. In this respect CCl_4 and SF_6 show the same behaviour. This is an interesting result pointing to the localized nature of the final states. Only if the final states are localized in the solid phase with little intermolecular overlap one might expect that molecular crystals show the same cross sections in gas and solid phase. Contrary to this situation we could show recently for small molecules like N_2 or CO_2 that strong band structure effects dominate the final states and the solid phase exhibits a completely different cross section than the gas phase. For both phases of CCl_4 the multiple scattering calculations by Grimm [23] seem to be able to explain at least qualitatively the cross section behaviour at low kinetic energies (E_{kin} < 15 eV) in terms of a large number of shape resonances.

Comparing the photoemission cross sections to x-ray absorption measurements [39-42], one would expect, as in the case of SF_6, to observe the same resonances. The only unambigously identified structure in the soft x-ray absorption spectrum is a discrete shape resonance about 5.4 - 7.2 eV below threshold, which is attributed to the $7a_1$ and $8t_2$ virtual orbitals. Above the thresholds for C 1s and Cl 1s, 2s, 2p excitation weak structures are observed of which some might be shape resonances. A clear identification and assignment is however still lacking.

If we think of shape resonances as being closely related to unoccupied molecular orbitals [12], it is tempting to set up an energetic scheme of the virtual orbitals for CCl_4. With the help of fig. 10, references [39-42] and on the basis of our measurements (see table 6) the ordering would be: $7a_1$, $8t_2$-(5.4-7.2 eV) ; 3e(2.2-2.7 eV) ; $3t_1$(2.3-2.7 eV) ; 4e(5.2 eV) ; $9t_2$(6.7 eV) ; $4t_1$(9.7-10.8 eV). The energies referred to the vacuum level are collected in table 7. One should of course be cautious with such a simple one electron scheme, because orbitals of the same symmetry are close together, e.g. 3e and 4e or $3t_1$ and $4t_1$ and it is not clear whether they can really be distinguished. It would be interesting to see if molecular orbital calculations are able to support our interpretation. Such calculations are not available at present.

Acknowledgement

We wish to thank Dipl.-Phys. F. Senf and H.-W. Biester for help with the experiments and stimulating discussions. We are grateful to the authors of references [23] and [25] for making available to us their results prior to publication. We would also like to acknowledge the continuous and efficient support of the technical staff of HASYLAB.

References

1 T.M. Zimkina and A.S. Vinogradov, J. Phys. (Paris) 32, C4-3 (1971)

2 J.L. Dehmer, J. Chem. Phys. 56, 4496 (1972)

3 D. Dill and J.L. Dehmer, J. Chem. Phys. 61, 692 (1974)

4 D. Loomba, S. Wallace, D. Dill and J.L. Dehmer, J. Chem. Phys. 75, 4546 (1981)

5 J.W. Davenport, PhD Thesis, University of Pennsylvania, 1976

6 J.L. Dehmer, D. Dill und A.C. Parr, Photoionization Dynamics of Small Molecules in S. McGlynn, G. Findley and R. Huebner (eds.), Photophysics and Photochemistry in the Vacuum Ultraviolet, D. Reidel Publishing Company, Dordrecht, Holland, 1983

7 A. Messiah, Quantenmechanik, Walter de Gruyter, Berlin, 1976, Band I, Kapitel 10.4

8 J.L. Dehmer, D. Dill and S. Wallace, Phys. Rev. Lett. 43, 1005 (1979)

9 J.R. Swanson, D. Dill and J.L. Dehmer, J. Phys. B 14, L207 (1981)

10 F.A. Grimm, J.D. Allen Jr., T.A. Carlson, M.O. Krause, D. Mehaffy, P.R. Keller and J.W. Taylor, J. Chem. Phys. 75, 92 (1981)

11 J.L. Dehmer and D. Dill, J. Chem. Phys. 65, 5327 (1981)

12 P.W. Langhoff, N. Padial, G. Csanak, T.N. Rescigno and B.V. McKoy, J. Chim. Phys. (Paris) 77, 589 (1980)

13 R.R. Lucchese and V. McKoy, J. Phys. Chem. 85, 2166 (1981)

14 G.J. Schulz, Rev. Mod. Phys. 45, 378 (1973)

15 R.E. Kennerly, Phys. Rev. A 21, 1876 (1980)

16 G.J. Schulz, A Review of Vibrational Excitation of Molecules by Electron Impact at Low Energies in G. Bekefi (ed.), Principles of Laser Plasmas, Wiley-Interscience, New York, 1976

17 J.L. Dehmer and D. Dill, Connections Between Molecular Photoionization and Electron-Molecule Scattering with Emphasis on Shape Resonances in I. Shimura and M. Matsuzawa, Symposium on Electron-Molecule Collisions, University of Tokyo, 1979

18 E.E. Koch and B.F. Sonntag, in C. Kunz (ed.), Topics in Current Physics, Vol. 10, Springer, Berlin, Heidelberg, New York, 1979, p. 269

19 D. Blechschmidt, R. Haensel, E.E. Koch, U. Nielsen and T. Sagawa, Chem. Phys. Lett. 14, 33 (1972)

20 H.J. Lau, J.-H. Fock and E.E. Koch, Chem. Phys. Lett. 89, 281 (1982)

21 J.-H. Fock, H.J. Lau and E.E. Koch, Chem. Phys. 83, 377 (1984)

22 J.-H. Fock and E.E. Koch, Chem. Phys. Lett. 105, 38 (1984)

23 F.A. Grimm, private communication

24 P.R. Keller, J.W. Taylor, T.A. Carlson and F.A. Grimm, Chem. Phys. 79, 269 (1983)

25 P.R. Keller, F.A. Grimm, T. Whitley, T.A. Carlson and J.W. Taylor, to be published

26 D. Briggs, R.A. Marbow and R.M. Lambert, Chem. Phys. Lett. 53, 462 (1978)

27 G. Rovida and F. Pratesi, Surf. Sci. 51, 270 (1975)

28 J.-H. Fock, PhD Thesis, University of Hamburg, 1983

29 K. Siegbahn, C. Nordling, A. Fahlmann, R. Nordberg, K. Hamrin, J. Hedmann, G. Johansson, T. Bergmark, S.-E. Karlsson, I. Lindgren and B. Lindberg, ESCA-Atomic, Molecular and Solid State Structure Studied by Means of Electron Spectroscopy, Almqvist & Wiksells, Uppsala, 1967

30 J.L. Dehmer, A.C. Parr, S. Wallace and D. Dill, J. Chem. Phys.

31 W.D. Grobman and E.E. Koch, in L. Ley and M. Cardona (eds.), Photoemission in Solids II, Topics in Applied Physics, Vol. 27, Springer, Berlin, Heidelberg, New York, 1979, p. 261

32 W.R. Salaneck, in D.W. Dwight, T.J. Fabish and H.R. Thomas (eds.), Photon Electron and Ion Probes of Polymer Structure and Properties, Am. Chem. Soc. Symposium Series, Vol. 162, Washington, 1981, p. 121

33 T. Gustafsson, Phys. Rev. A 18, 1481 (1978)

34 J.L. Dehmer, J. Siegel and D. Dill, J. Chem. Phys. 69, 5205 (1978)

35 R.E. Kennerly, R.A. Bonham and M. McMillian, J. Chem. Phys. 70, 2039 (1979)

36 H.J. Levinson, T. Gustafsson and P. Soven, Phys. Rev. A 19, 1089 (1979)

37 J.R. Swanson, D. Dill and J.L. Dehmer, J. Phys. B 13, L231 (1980)

38 R.S. Wallace, PhD Thesis, Boston University, 1980

39 A.P. Sadovskii, V.M. Bertenev and S.M. Blokhin, Theor. Exp. Chem. 4, 342 (1968)

40 A.P. Hitchcock and C.E. Brion, J. Elec. Spec. 14, 417 (1978)

41 V.N. Sivkov, V.N. Akimov, A.S. Vinogradov and T.M. Zimkina, preliminary data, unpublished, 1982

42 G. O'Sullivan, J. Phys. b 15, 2385 (1982)

43 T.A. Carlson, M.O. Krause, F.A. Grimm, P. Keller and J.W. Taylor, J. Chem. Phys. 77, 5340 (1982)

44 K. Kimura, S. Katsumata, Y. Achiba, T. Yamazaki and S. Iwata, Handbook on HeI Photoelectron Spectra of Fundamental Organic Molecules, Japan Scientific Societies Press, Tokyo, 1981

45 A.W. Potts, H.J. Lempka, D.G. Streets and W.C. Price, Phil. Trans. Roy. Soc. London A 268, 59 (1970)

46 L. Karlson, L. Mattson, R. Jadrny, T. Bergmark and K. Siegbahn, Physica Scripta 14, 230 (1976)

Table 1

Vertical (IP_{vert}) and adiabatic (IP_{ad}) ionization potentials, full width half maximum (fwhm) and energy shift between gas phase and solid SF_6. For the solid phase the adiabatic potential has been determined according to the formula $IP_{ad} = IP_{vert} - (1{,}2 \times fwhm)$. All values are in eV, the errors for the solid phase data are ≈ 0.1 eV.

Initial Orbital	solid (this work)			Gas (a)		Shift	
	IP_{vert}	fwhm	IP_{ad}	IP_{vert}	IP_{ad}	IP_{vert}	IP_{ad}
$1t_{1g}$	15,08	0,67	14,3	15,67	15,5	0,59	1,2
$5t_{1u}$ $+1t_{2u}$	16,40	0,92	15,3	16,93	16,7	0,53	1,4
$3e_g$	17,82	0,73	16,9	18,3	18,0	0,48	1,1
				18,66		0,84	
$1t_{2g}$	19,15	1,05	17,9	19,758	19,245	0,61	1,3
$4t_{1u}$	21,91	0,76	21,0	22,7	-	0,79	-
$5a_{1g}$	26,16	0,74	25,3	27,0	-	0,84	-

(a) Ref. 44

Table 2

Summary of observed features in photoemission cross sections for gaseous and solid SF_6. All energies in eV. Values in brackets designate observed shoulders.

Orbital	solid (this work)		Gas (a)		Gas (b)		Assignment
	hν	E_{kin}	hν	E_{kin}	hν	E_{kin}	
$1t_{1g}$	17,0	1,9	-	-	17,0	1,3	$1t_{1g} \rightarrow 6t_{1u}$
	20,0	4,9	-	-	20,0	4,3	
	23,0	7,9	23,0	7,3	24,0	8,3	
	27,0	11,9	-	-	-	-	
	29,0	13,9	29,0	13,3	-	-	
$5t_{1u}$ $+1t_{2u}$	20,0	3,6	18,5	1,6	18,0	1,1	$5t_{1u} \rightarrow 2t_{2g}$ / $1t_{2u} \rightarrow 2t_{2g}$
	23,0	6,6	22,5	5,6	23,0	6,1	
	29,0	12,6	(29,0	12,1)	-	-	
$3e_g$	(20,0	2,2)	20,0	1,5	19,0	0,5	$3e_g \rightarrow 6t_{1u}$
	22,5	4,7	23,0	4,5	23,5	5,0	
	26,5	8,7	-	-	-	-	
$1t_{2g}$	22,5	3,4	22,5	2,7	23,0	3,2	$1t_{2g} \rightarrow 6t_{1u}$
	27,0	7,9	-	-	-	-	
$4t_{1u}$	23,5	1,6	23,0	0,3	24,0	1,3	
	28,0	6,1	28,0	5,3	28,0	5,3	$4t_{1u} \rightarrow 2t_{2g}$
	(30.0	8.1)	-	-	-	-	

(a) Ref. 33

(b) Ref. 30

Table 3

Shape resonances for SF_6 observed in X-ray absorption A [2] and electron scattering B [34,35]. The minus sign in X-ray absorption indicates that the resonances occur in the discrete part of the spectrum below threshold.

Final orbital symmetry	E_{kin} (eV) A	B	E_{kin} (ev) A-B	Partial waves
$6a_{1g}$	-9,6	2,56	-12,2	0,4
$6t_{1u}$	-3,3	7,05	-10,4	1,3
$2t_{2g}$	+2,8	11,87	- 9,1	2,4,6
$4e_g$	+15,3	(25-55)	-(10-40)	2,4,6

Table 4

Vertical (IP_{vert}) and adiabatic (IP_{ad}) ionization potentials, full width half maximum (fwhm) and energy shift between gas phase and solid CCl_4. For the solid phase the adiabatic potential has been determined according to the formula $IP_{ad} = IP_{vert} - (1.2 \times fwhm)$. All values are in eV, the errors for the solid phase data are ≈ 0.1 eV.

Initial orbital	solid (this work)			Gas (a,b)		Shift
	IP_{vert}	fwhm	IP_{ad}	IP_{vert}	IP_{ad}	IP_{vert}
$2t_1$	10,27	0,76	9,4	11,69	-	1,42
$7t_2$	11,27	1,31	9,7	12,62	-	1,35
$2e$	12,22	0,53	11,6	13,44	-	1,22
$6t_2$	15,26	0,70	14,4	16,58	-	1,32
$6a_1$	18,66	0,99	17,5	20,00	-	1,34

(a) Ref. 44

(b) Ref. 45

Table 5

Allowed dipole-transitions for the valence MO's of CCl_4.

$2t_1$ →	a_2	e	t_1	t_2
$7t_2$ → a_1		e	t_1	t_2
2e →			t_1	t_2
$6t_2$ → a_1		e	t_1	t_2
$6a_1$ →				t_2

Table 6

Summary of observed and calculated features in photoemission cross sections for gaseous and solid CCl_4. All energies are in eV.

Orbital	solid (this work)		Gas (theory,a)	Assignment
	$h\nu$	E_{kin}	E_{kin}	
$2t_1$	13,0	2,7	2,4	$2t_1 \rightarrow 3t_1$
	15,5	5,2	2,4	$2t_1 \rightarrow 3e$
$7t_2$	13,5	2,2	4,4	$7t_2 \rightarrow 4e$
	18,0	6,7	6,4	$7t_2 \rightarrow 9t_2$
2e	14,5	2,3	2,6	$2e \rightarrow 3t_1$
	23,0	10,8	8,6	$2e \rightarrow 4t_1$
$6t_2$	18,0	2,7	2,4	$6t_2 \rightarrow 3e$
	(25,0)	(9,7)	8,4	$6t_2 \rightarrow 4t_1$

(a) Ref. 23

Table 7

Proposed ordering and assignments of virtual orbitals for CCl_4. All energies are in eV referenced to the vacuum level (i.e. negative values are below the vacuum level). For details see text.

Energy	Assignment
(-7.2) - (-5.4)	$7a_1$, $8t_2$
2.2 - 2.7	3e
2.3 - 2.7	$3t_1$
5.2	4e
6.7	$9t_2$
9.7 - 15.8	$4t_1$

APPENDIX

Table A1

Relative cross section data for solid SF_6 plotted in figs. 5 and 6. The weighting factor is due to different pass energies of the electron analyzer.

hν	weighting factor	Relative cross sections $1t_{1g}$	$1t_{2u} + 5t_{1u}$	$3e_g$	$1t_{2g}$	$4t_{1u}$	
15.00	1	0.22					
15.50	1	0.79					
16.00	1	2.42	0.67				
16.50	1	5.56	2.84				
17.00	1	5.87	5.56				
17.50	1	4.90	8.78	0.09			
18.00	1	4.11	11.05	0.78			
18.50	1	2.29	13.70	2.03			
19.00	1	2.14	14.70	4.48	0.14		
19.50	1	2.89	14.30	6.22	0.56		
20.00	1	3.25	16.30	5.12	2.35		
20.50	1	3.02	15.10	7.62	3.55		
21.00	1	2.93	14.10	8.00	5.78		
21.50	1	3.57	16.50	9.30	6.17		
22.00	1	4.48	19.30	7.61	10.82	0.61	
22.50	1	5.79	21.15	10.19	10.10	0.55	
23.00	1	7.09	22.50	8.48	10.16	1.19	
23.50	1	6.77	21.30	6.76	6.42	2.02	
24.00	1	5.61	20.10	4.51	5.89	1.98	
24.50	1	4.92	18.40	4.30	4.30	1.94	
25.00	4.18	18.88	71.26	13.25	16.82	7.86	
25.50	4.18	20.46	64.48	13.26	18.15	7.42	
26.00	4.18	26.12	54.32	12.71	19.48	5.93	
26.50	4.18	29.10	37.48	15.92	17.86	5.67	
27.00	4.18	28.20	28.91	13.30	17.77	7.15	
27.50	4.18	25.92	25.30	7.49	15.48	12.06	
28.00	4.18	25.81	25.38	4.11	13.17	17.49	
28.50	4.18	26.43	25.89	2.98	9.44	14.60	
29.00	4.18	24.73	28.84	3.11	6.96	11.64	
29.50	4.18	21.84	22.63	3.27	5.75	11.01	
30.00	4.18	19.91	21.18	3.14	5.80	10.29	
31.00	8.8	38.74	39.02	7.69	13.75	15.26	
32.00	8.8	30.79	31.83	6.61	13.12	4.52	
33.00	8.8	24.30	26.41	5.49	10.82	5.76	
34.00	8.8	23.24	27.88	5.70	11.84	8.37	
35.00	16.7	37.30	42.50	10.90	19.80	13.10	
36.00	16.7	35.40	38.50	11.60	20.00	13.10	
37.00	16.7	30.30	28.50	11.20	15.80	11.90	2.50
38.00	16.7	26.00	22.50	10.30	12.00	10.90	7.30
39.00	16.7	22.20	19.70	9.00	9.80	11.10	6.90
40.00	16.7	15.30	13.20	6.70	5.28	8.36	5.16

Table A2

Branching ratio for solid SF_6 as plotted in fig. 7.

hν (eV)	Branching ratio					
	$1t_{1g}$	$1t_{2u} + 5t_{1u}$	$3e_g$	$1t_{2g}$	$4t_{1u}$	$5a_{1g}$
15.00	1.000					
15.50	1.000					
16.00	0.783	0.217				
16.50	0.662	0.338				
17.00	0.514	0.486				
17.50	0.356	0.638	0.006			
18.00	0.258	0.693	0.049			
18.50	0.127	0.760	0.113			
19.00	0.100	0.685	0.209	0.006		
19.50	0.121	0.597	0.259	0.023		
20.00	0.120	0.603	0.190	0.087		
20.50	0.103	0.516	0.260	0.121		
21.00	0.099	0.456	0.258	0.187		
21.50	0.101	0.464	0.262	0.174		
22.00	0.105	0.451	0.178	0.253	0.014	
22.50	0.122	0.447	0.216	0.011	0.011	
23.00	0.144	0.455	0.172	0.206	0.024	
23.50	0.156	0.492	0.156	0.148	0.047	
24.00	0.148	0.528	0.119	0.155	0.052	
24.50	0.145	0.543	0.127	0.127	0.057	
25.00	0.148	0.553	0.104	0.133	0.063	
25.50	0.165	0.521	0.107	0.147	0.060	
26.00	0.207	0.458	0.107	0.164	0.050	
26.50	0.274	0.354	0.151	0.169	0.054	
27.00	0.296	0.304	0.140	0.186	0.075	
27.50	0.301	0.293	0.087	0.179	0.140	
28.00	0.300	0.295	0.048	0.153	0.203	
28.50	0.330	0.327	0.038	0.119	0.184	
29.00	0.347	0.349	0.044	0.098	0.163	
29.50	0.338	0.351	0.050	0.090	0.171	
30.00	0.335	0.351	0.052	0.094	0.167	
31.00	0.339	0.341	0.067	0.120	0.134	
32.00	0.354	0.366	0.076	0.151	0.052	
33.00	0.334	0.363	0.075	0.149	0.079	
34.00	0.301	0.363	0.074	0.154	0.109	
35.00	0.299	0.347	0.087	0.161	0.108	
36.00	0.299	0.325	0.098	0.169	0.111	
37.00	0.302	0.284	0.112	0.158	0.119	0.025
38.00	0.292	0.253	0.116	0.135	0.122	0.082
39.00	0.282	0.250	0.114	0.124	0.141	0.088
40.00	0.283	0.244	0.124	0.098	0.155	0.096

Table A3

Relative cross section data for solid CCl_4 plotted in fig. 13. The weighting factor is due to different pass energies of the electron analyzer.

hν (eV)	weighting factor	Relative cross section				
		$2t_1$	$7t_2$	$3e$	$6t_2$	$6a_1$
10.50	1	0.77				
11.00	1	2.68				
11.50	1	7.50				
12.00	1	9.10	5.75			
12.50	1	12.47	7.93			
13.00	1	12.75	9.79	0.05		
13.50	1	12.26	10.26	1.38		
14.00	1	11.18	9.76	1.54		
14.50	1	10.04	9.41	1.73		
15.00	1	9.86	9.05	1.39		
15.50	1	9.85	8.93	1.60	0.47	
16.00		9.63	8.86	1.52	0.94	
16.50	1	9.65	9.11	1.56	2.58	
10.00	1	8.89	8.88	1.58	4.22	
17.50	1	8.19	8.95	1.17	4.92	
18.00	1	7.48	8.08	1.16	5.06	
18.50	1	6.38	8.55	1.02	5.00	
19.00	1	6.35	7.68	1.08	4.38	
19.50	1	4.75	6.86	0.92	3.70	
20.00	1	3.94	6.19	0.96	3.38	
20.50	1				3.17	
21.00	1	2.98	5.23	1.03	2.68	
21.50	1				2.41	
22.00	1	2.65	4.73	1.09	2.32	
22.50	1				2.15	
23.00	1	2.23	3.80	1.10	2.07	0.89
23.50	1				1.90	
24.00	1	1.72	3.04	0.95	1.86	
24.50	1	1.78	2.64	1.08	1.83	0.80
25.00	1	1.49	2.26	0.92	1.70	0.74
26.00	2.45	2.78	4.04	1.73	2.97	1.08
27.00	2.45	2.34	3.47	1.51	2.69	1.18
28.00	2.45	1.86	2.90	1.28	2.19	0.69
29.00	2.45	1.65	2.20	1.02	1.83	0.52
30.00	2.45	1.16	1.63	0.74	1.40	0.39

Table A4

Branching ratios for solid CCl_4 as plotted in fig. 14.

hν (eV)	Branching ratio $2t_1$	$7t_2$	2e	$6t_2$	$6a_1$
10.50	1.000				
11.00	1.000				
11.50	1.000				
12.00	0.613	0.387			
12.50	0.611	0.389			
13.00	0.564	0.433	0.002		
13.50	0.513	0.429	0.058		
14.00	0.497	0.434	0.068		
14.50	0.474	0.444	0.082		
15.00	0.486	0.446	0.068		
15.50	0.472	0.428	0.077	0.022	
16.00	0.460	0.423	0.073	0.045	
16.50	0.421	0.398	0.068	0.113	
17.00	0.377	0.377	0.067	0.179	
17.50	0.353	0.385	0.050	0.199	
18.00	9,343	0,371	0.053	0.232	
18.50	0.305	0.408	0.049	0.239	
19.00	0.326	0.394	0.055	0.225	
19.50	0.293	0.422	0.057	0.228	
20.00	0.272	0.429	0.067	0.234	
21.00	0.250	0.440	0.086	0.225	
22.00	0.246	0.439	0.102	0.215	
23.00	0.221	0.377	0.109	0.205	0.088
24.00	0.203	0.359	0.112	0.213	0.108
24.50	0.219	0.318	0.130	0.232	0.101
25.00	0.207	0.323	0.129	0.234	0.107
26.00	0.221	0.321	0.137	0.236	0.086
27.00	0.209	0.310	0.135	0.240	0.106
28.00	0.209	0.325	0.144	0.245	0.077
29.00	0.229	0.305	0.141	0.253	0.072
30.00	0.218	0.306	0.139	0.263	0.073

Figure Captions

Fig. 1 Schematic representation of the effective molecular potential and the different types of molecular orbitals (from Ref. [18]).

Fig. 2 Molecular orbital scheme for SF_6. The approximate binding energies are taken from UPS and XPS data [2,29,44] for gaseous SF_6 and are refered to the vacuum level. On the right hand side photoelectron spectra for SF_6 are plotted.

Fig. 3 Comparison of the gas-phase photoelectron spectrum from Ref. [46] (upper panel) with a photoelectron-energy distribution curve for solid SF_6 (this work, lower panel). Both spectra are plotted on the same binding energy scale with the vacuum level $E_{vac} = 0$. The valence molecular orbitals are denoted by the one-electron MO notation. The deconvolution of the EDC for solid SF_6 into seven bands is also shown. Crosses give the measured EDC while the solid line gives the sum of the individual bands.

Fig. 4 Photoelectron-energy distribution curves for polycrystalline solid SF_6 for excitation energies ranging between 16 eV and 40 eV. In this plot the same initial states follow inclined lines.

Fig. 5 Relative partial ionization cross sections for the $1t_{1g}$ derived and $1t_{2u} + 5t_{1u}$ derived valence bands of solid SF_6 (crosses). The arrows mark the onset for photoemission from these bands. For comparison the gas phase partial cross sections are also shown (full circles, Ref. [33], open circles Ref. [30]).

Fig. 6 Relative partial ionization cross sections for the $3e_g$, $1t_{2g}$, $4t_{1u}$, and $5a_{1g}$ derived valence bands of solid SF_6. The arrows mark the onset for photoemission from these bands. For $5a_{1g}$ with a threshold at 26.16 eV only four data points could be measured at $h\nu \geq 37$ eV. For comparison the gas phase partial cross sections are also shown (full circles Ref. [33], open circles Ref. [30]). The relative scale is the same in figs. 5 and 6.

Fig. 7 Branching ratios for the one-electron states of solid SF_6.

Fig. 8 Plot of shape resonances observed for SF_6 in X-ray absorption [2], gas-phase, and solid-phase photoelectron spectroscopy and in electron scattering [34,35]. The zero of the energy scale denotes the vacuum level or ionization threshold. Negative energies denote "discrete shape resonances" below threshold.

Fig. 9 Comparison of the optical VUV spectrum (reflectivity spectrum which in this case closely resembles the dielectric function ε_2) of solid SF_6 [19] with the partial and summed photoionization cross sections as determined in this work.

Fig. 10 Molecular orbital scheme for CCl_4 (center) build from the C and the Cl atomic orbitals in the T_d field.

Fig. 11 Photoelectron-energy distribution curves for polycrystalline solid CCl_4 for excitation energies ranging from 11 to 30 eV. In this plot the same initial states follow inclined lines. The five valence molecular orbitals are denoted by the one electron MO notation.

Fig. 12 Comparison of the gas-phase photoelectron spectrum from Kimura et al. [44] (upper curve) with a photoelectron-energy distribution curve for solid CCl_4 (this work, lower curve). The binding energy scale refers to the spectrum of solid CCl_4 with $E_{vac} = 0$. The gas phase spectrum has been shifted rigidly by the relaxation energy $\Delta E_R^{vert} = 1.3$ eV in order to obtain an alignment of the prominent features. The deconvolution of the EDC for solid CCl_4 into four bands is also shown. Crosses give the measured EDC while the solid line gives the sum of the individual bands.

Fig. 13 Relative partial ionization cross sections for the $2t_1$, $7t_2$, 2e, $6t_2$, and $6a_1$ derived valence bands of solid CCl_4. The arrows mark the onset for photoemission from these bands.

Fig. 14 Branching ratios for the one-electron states of solid CCl_4.

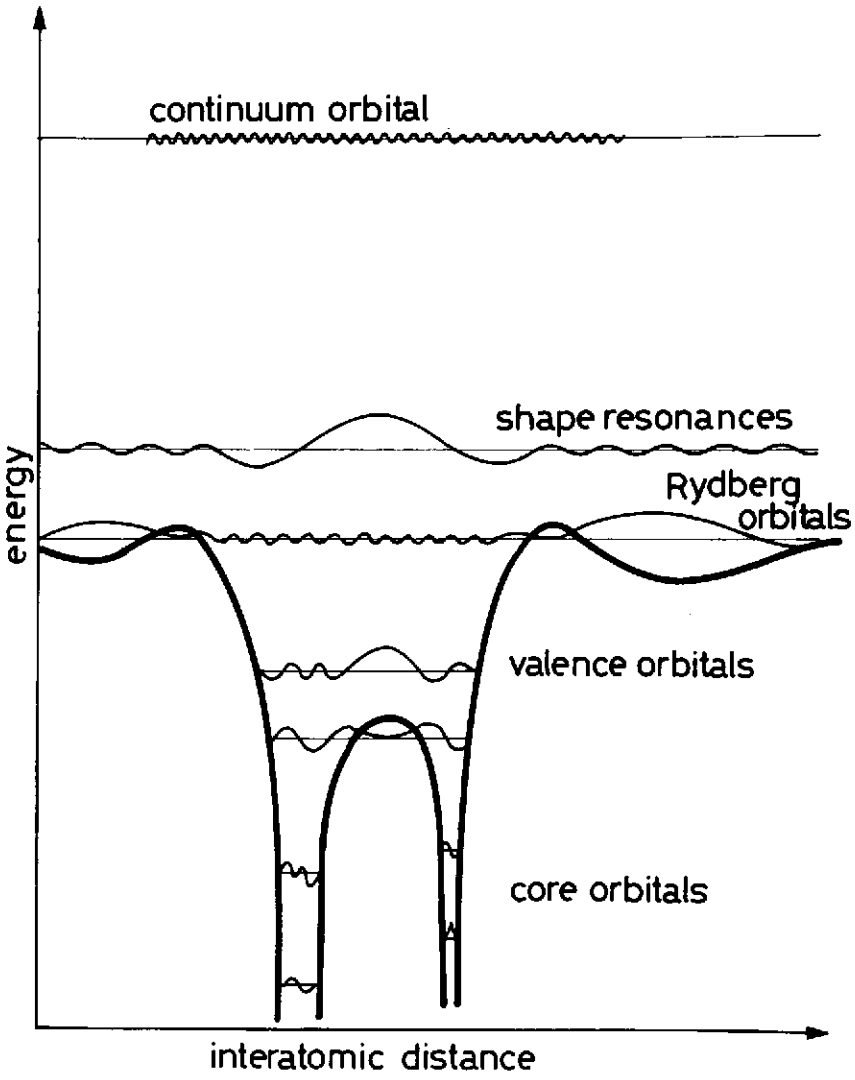

Fig. 1

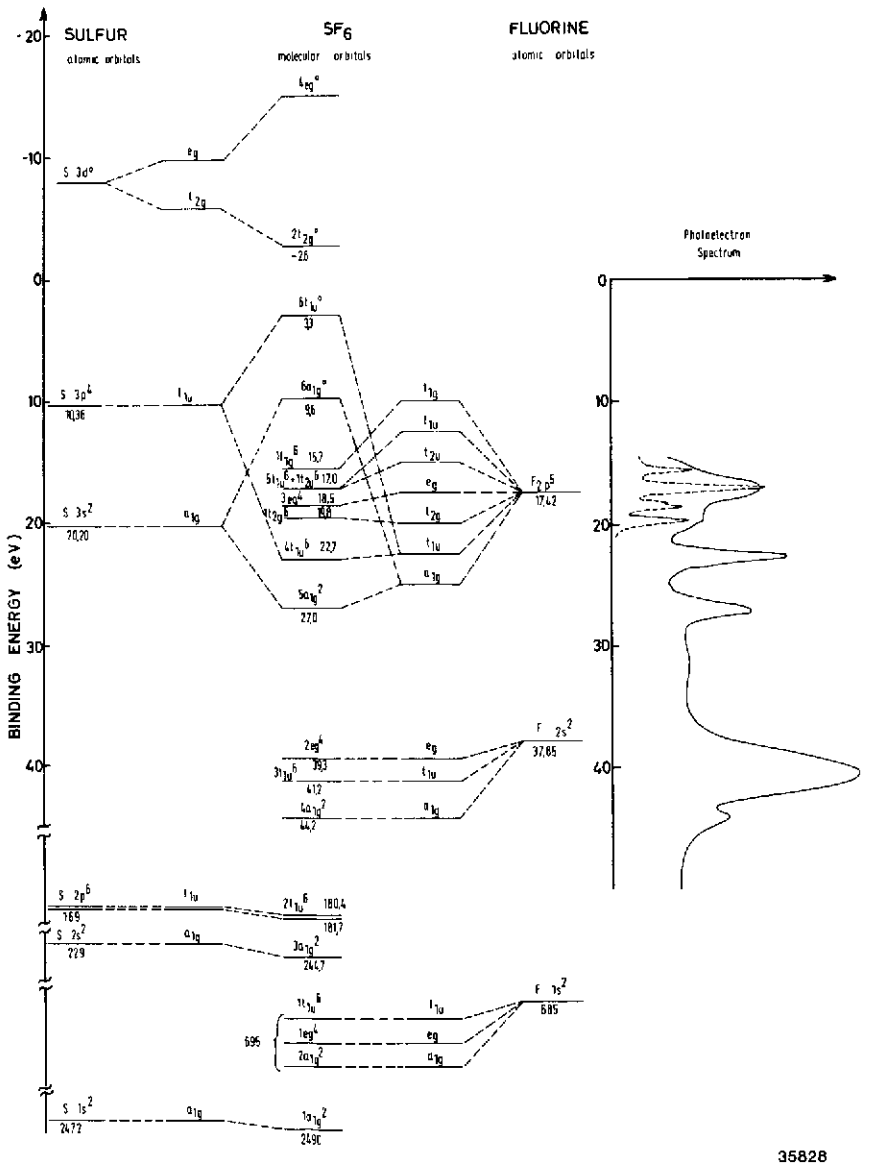
SULFUR
atomic orbitals
SF6
molecular orbitals
FLUORINE
atomic orbitals
Photoelectron Spectrum
BINDING ENERGY (eV)
35828

Fig. 2

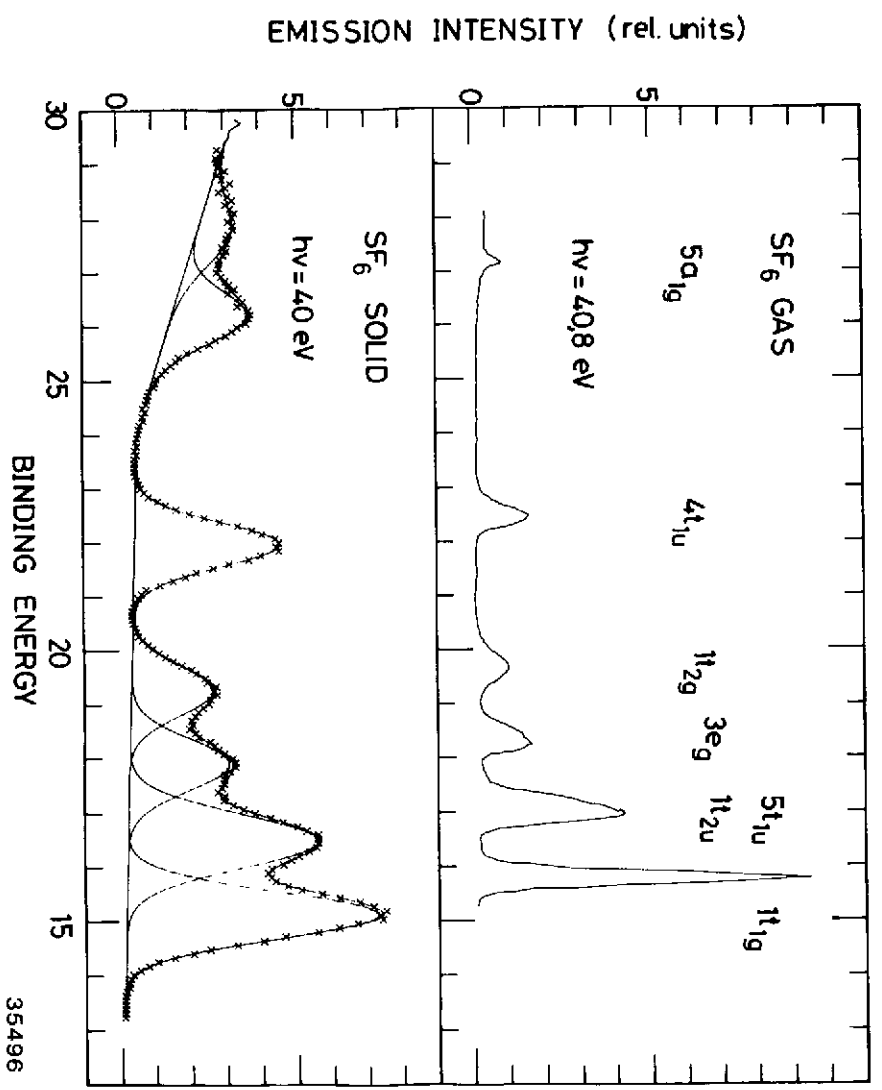
EMISSION INTENSITY (rel. units)
SF6 GAS
hν = 40,8 eV
SF6 SOLID
hν = 40 eV
BINDING ENERGY
35496

Fig. 3

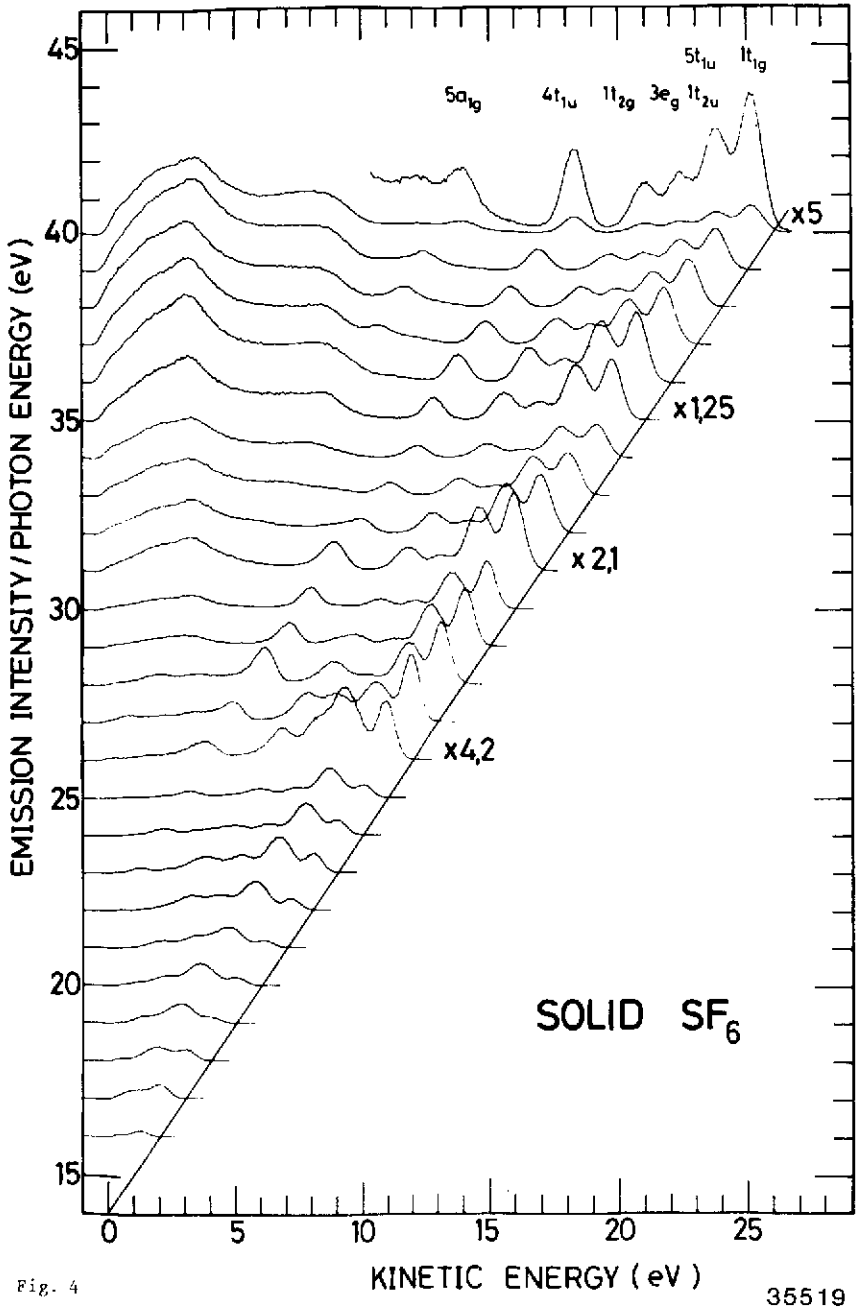
EMISSION INTENSITY / PHOTON ENERGY (eV)
KINETIC ENERGY (eV)
5a1g
4t1u
1t2g
3eg
1t2u
5t1u
1t1g
x5
x1,25
x 2,1
x4,2
SOLID SF6
35519

Fig. 4

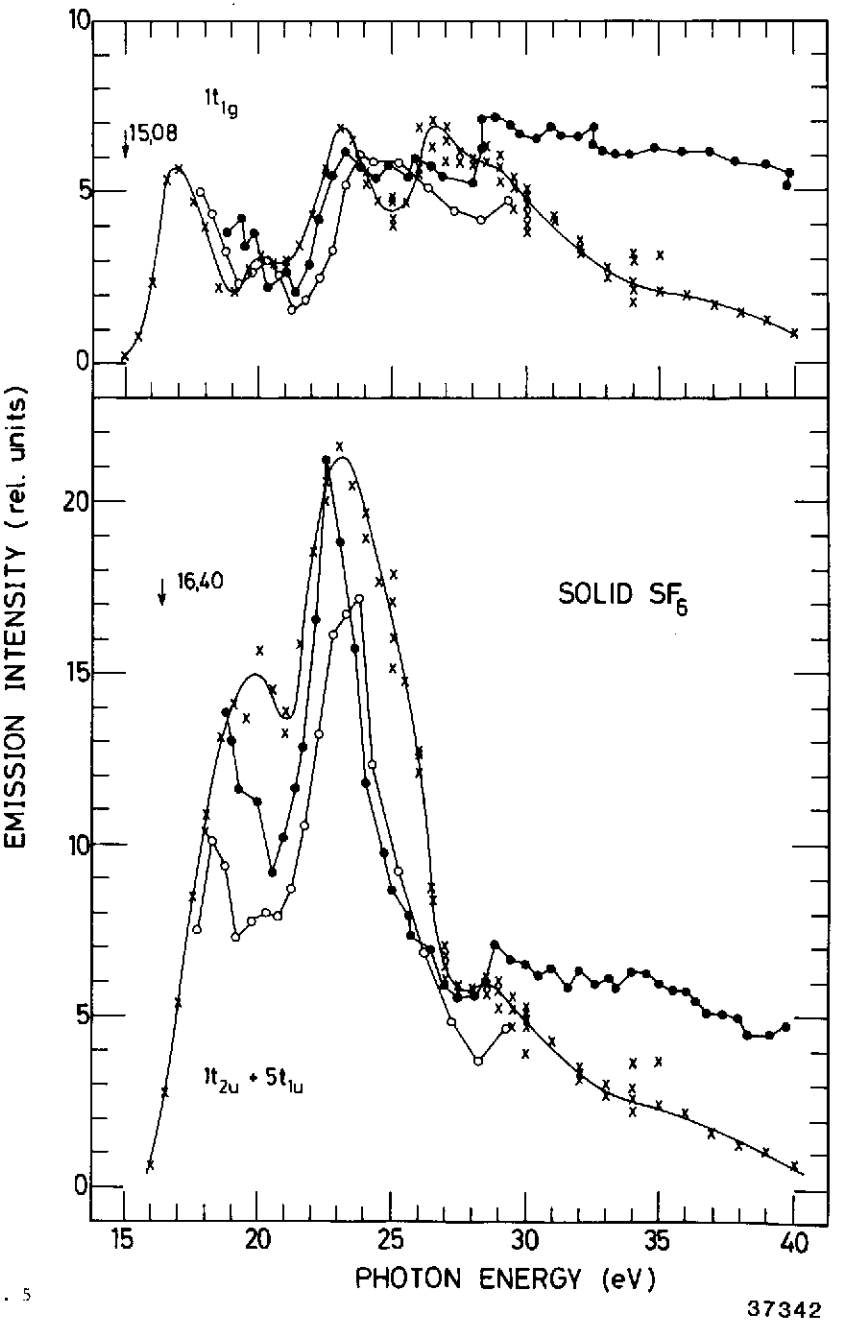
EMISSION INTENSITY (rel. units)
PHOTON ENERGY (eV)
1t1g
15,08
16,40
SOLID SF6
1t2u + 5t1u
37342

Fig. 5

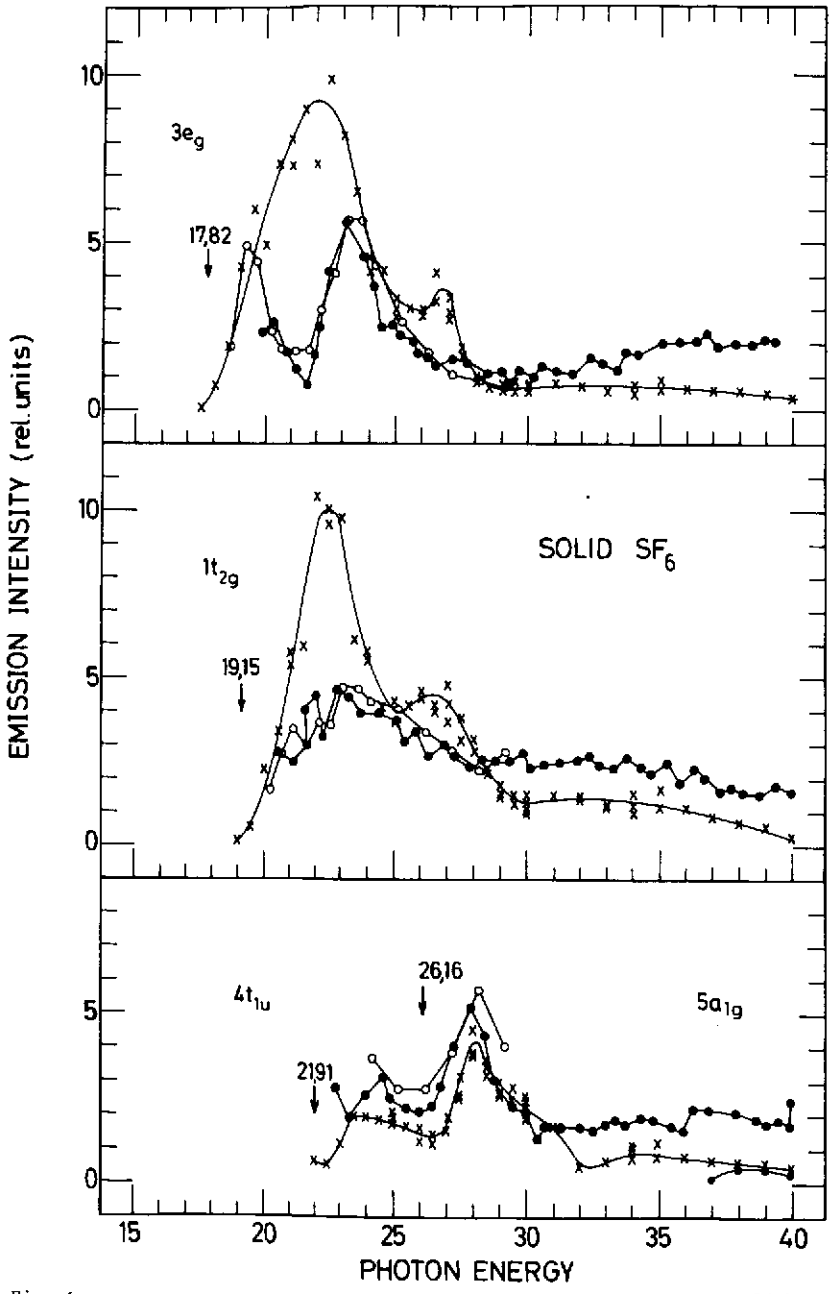
EMISSION INTENSITY (rel.units)
3e_g
17,82
SOLID SF_6
1t_2g
19,15
4t_1u
26,16
5a_1g
21,91
PHOTON ENERGY
37341

Fig. 6

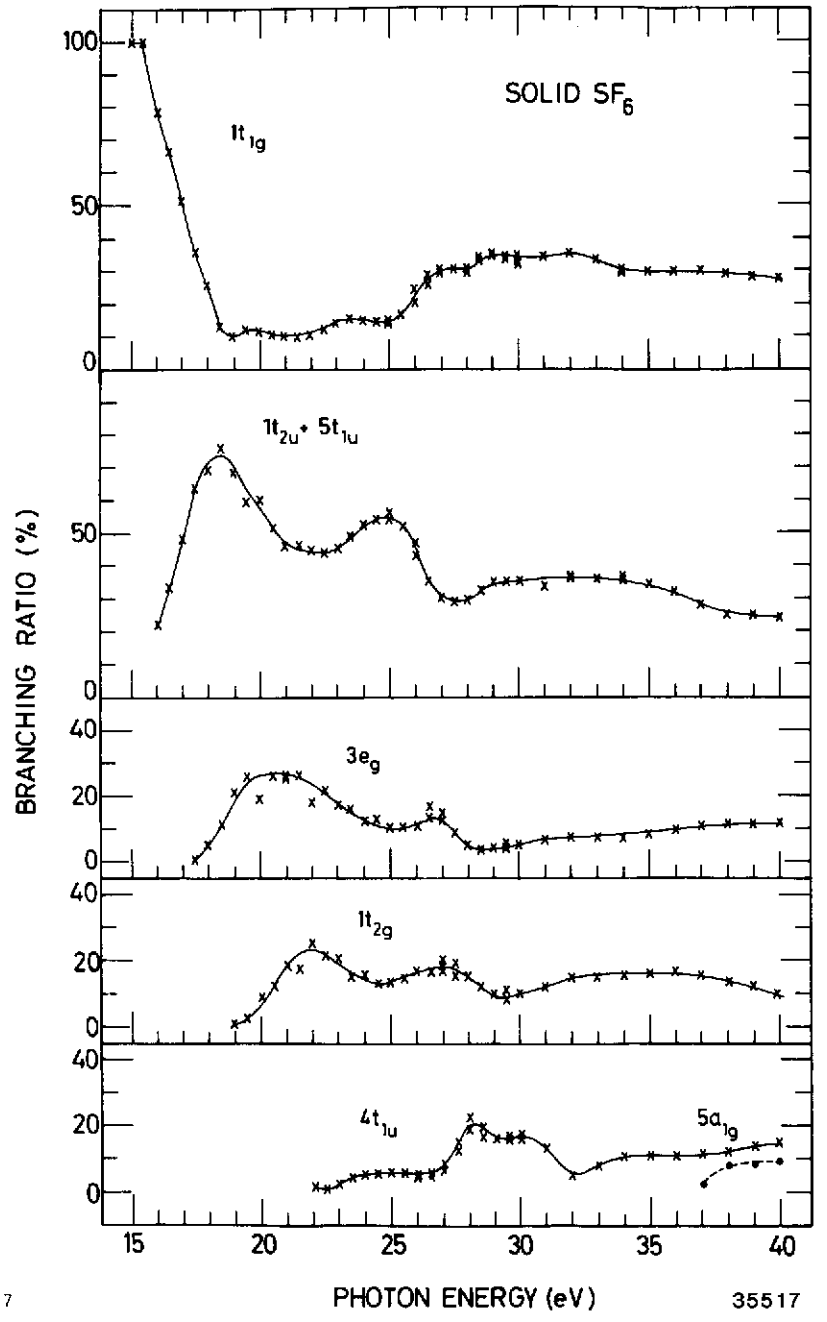
BRANCHING RATIO (%)
SOLID SF_6
1t_1g
1t_2u + 5t_1u
3e_g
1t_2g
4t_1u
5a_1g
PHOTON ENERGY (eV)
35517

Fig. 7

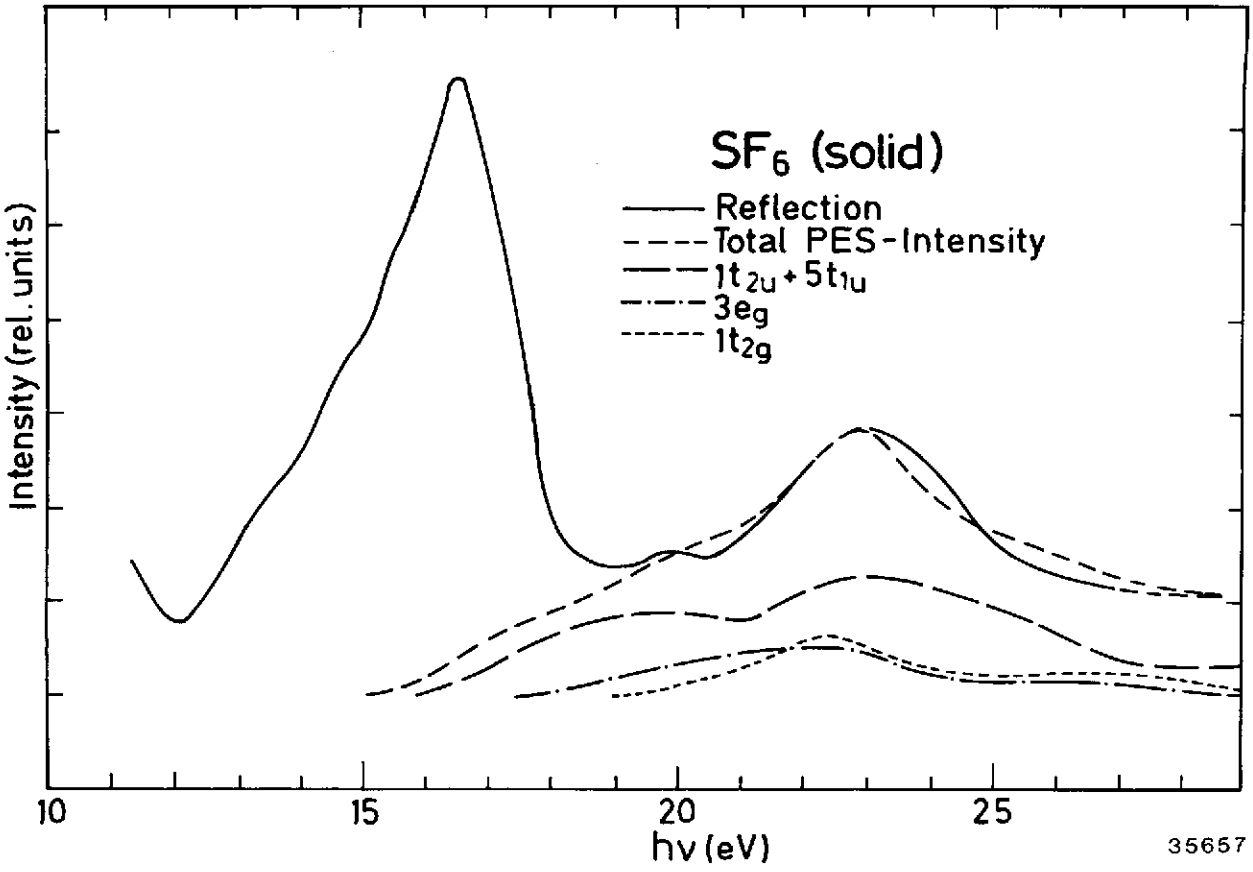
SF6 (solid)
Reflection
Total PES-Intensity
1t2u + 5t1u
3eg
1t2g
Intensity (rel. units)
10
15
20
25
hν (eV)
35657

Fig. 9

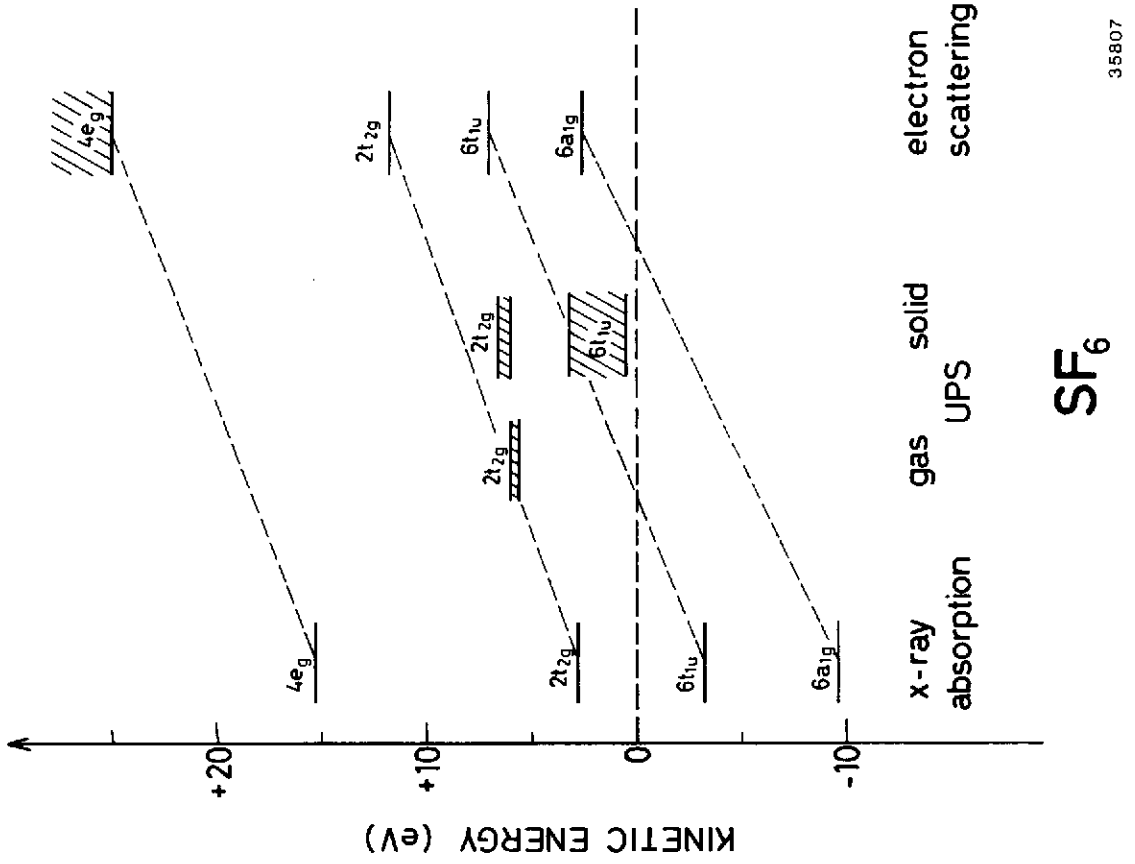
SF6
electron scattering
solid
gas
UPS
x-ray absorption
4eg
2t2g
6t1u
6a1g
+20
+10
0
-10
KINETIC ENERGY (eV)
35807

Fig. 8

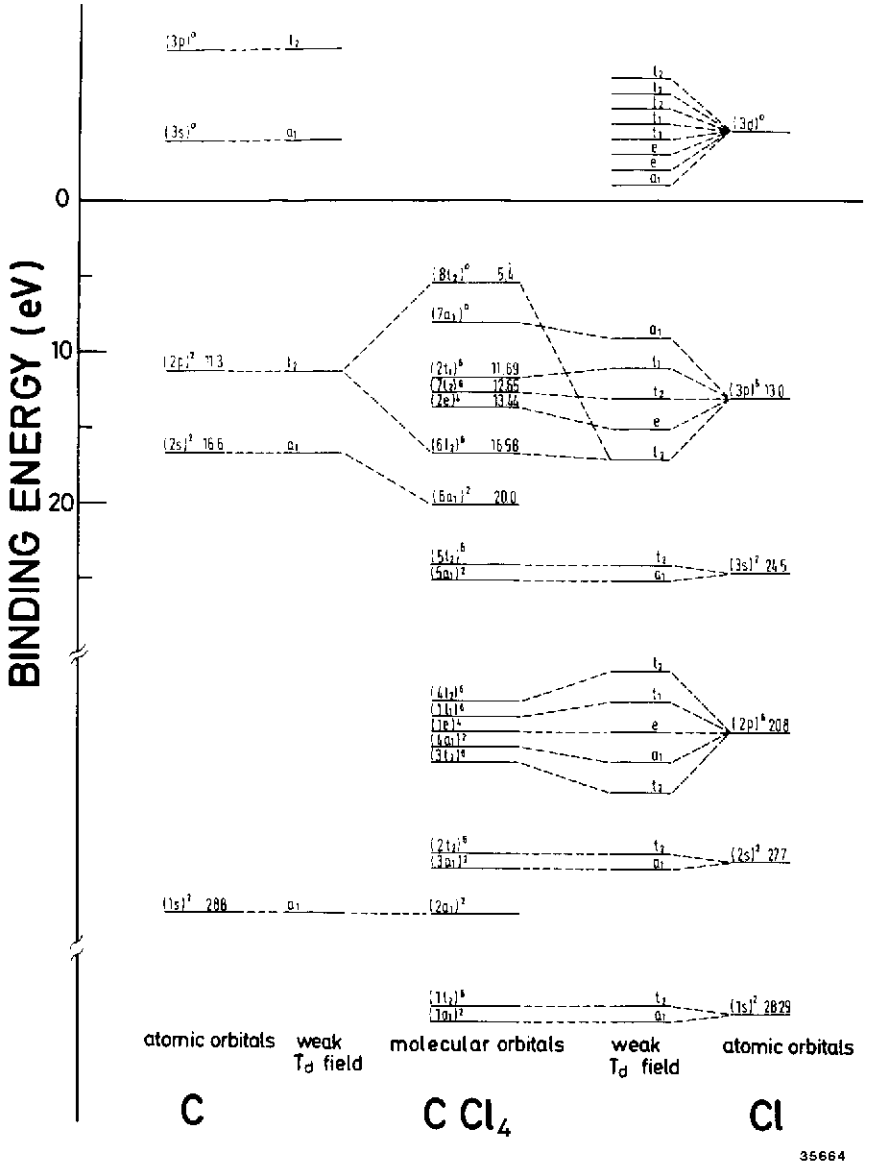
BINDING ENERGY (eV)
0
10
20
atomic orbitals
weak
T_d field
molecular orbitals
weak
T_d field
atomic orbitals
C
C Cl_4
Cl
35664

Fig. 10

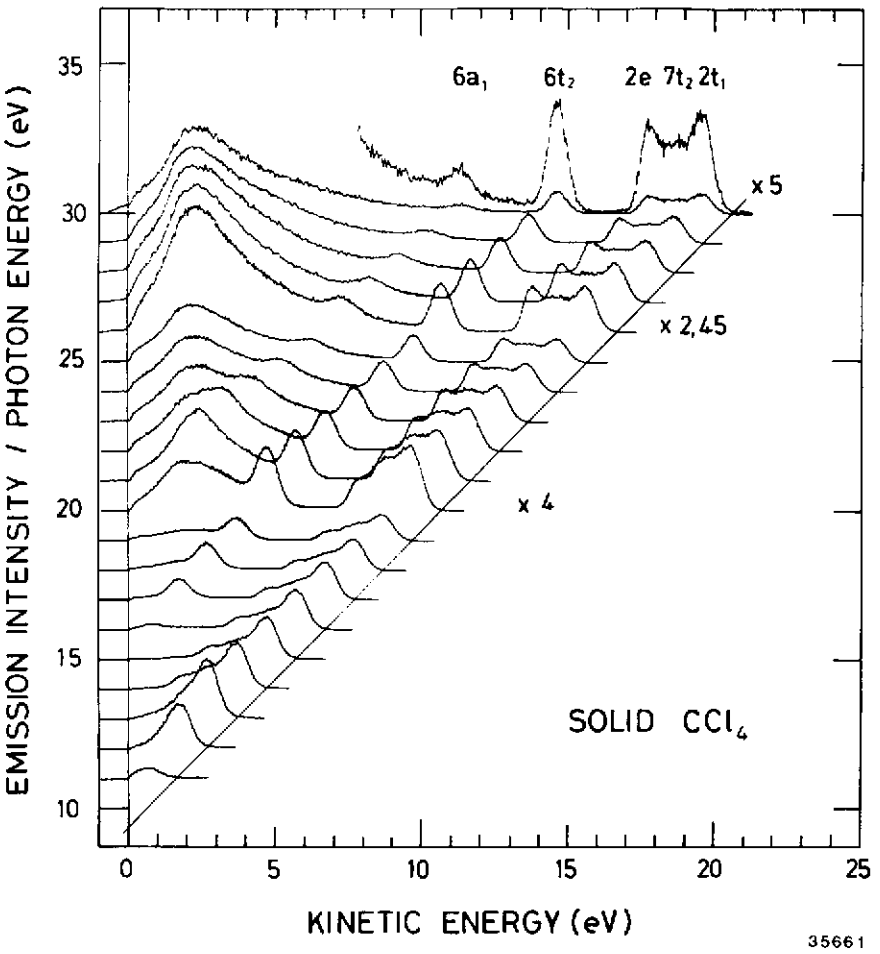
EMISSION INTENSITY / PHOTON ENERGY (eV)
KINETIC ENERGY (eV)
$6a_1$
$6t_2$
2e $7t_2$ $2t_1$
x 5
x 2,45
x 4
SOLID CCl_4
35661

Fig. 11

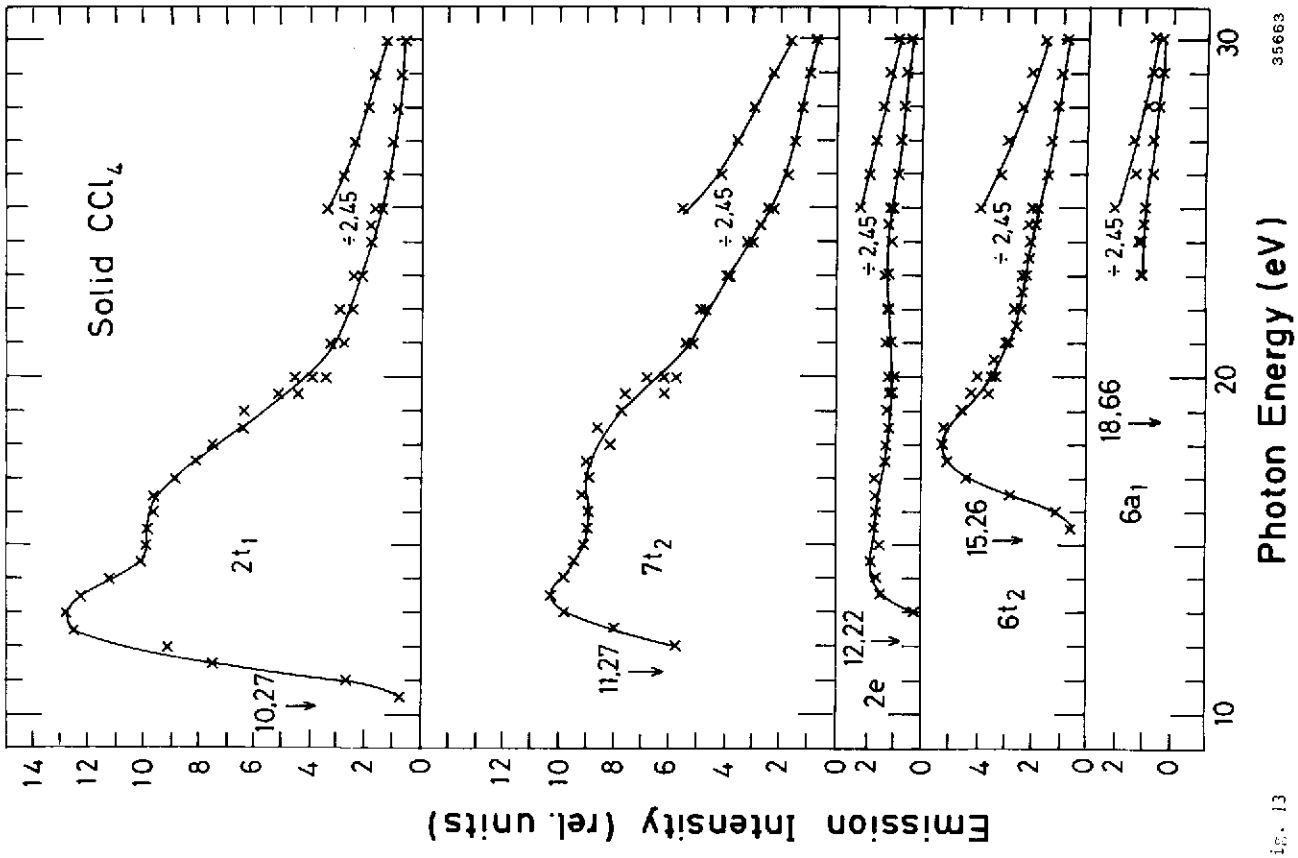
Solid CCl_4
÷2,45
$2t_1$
10,27
$7t_2$
11,27
2e
12,22
$6t_2$
15,26
$6a_1$
18,66
Emission Intensity (rel. units)
Photon Energy (eV)
35663

Fig. 13

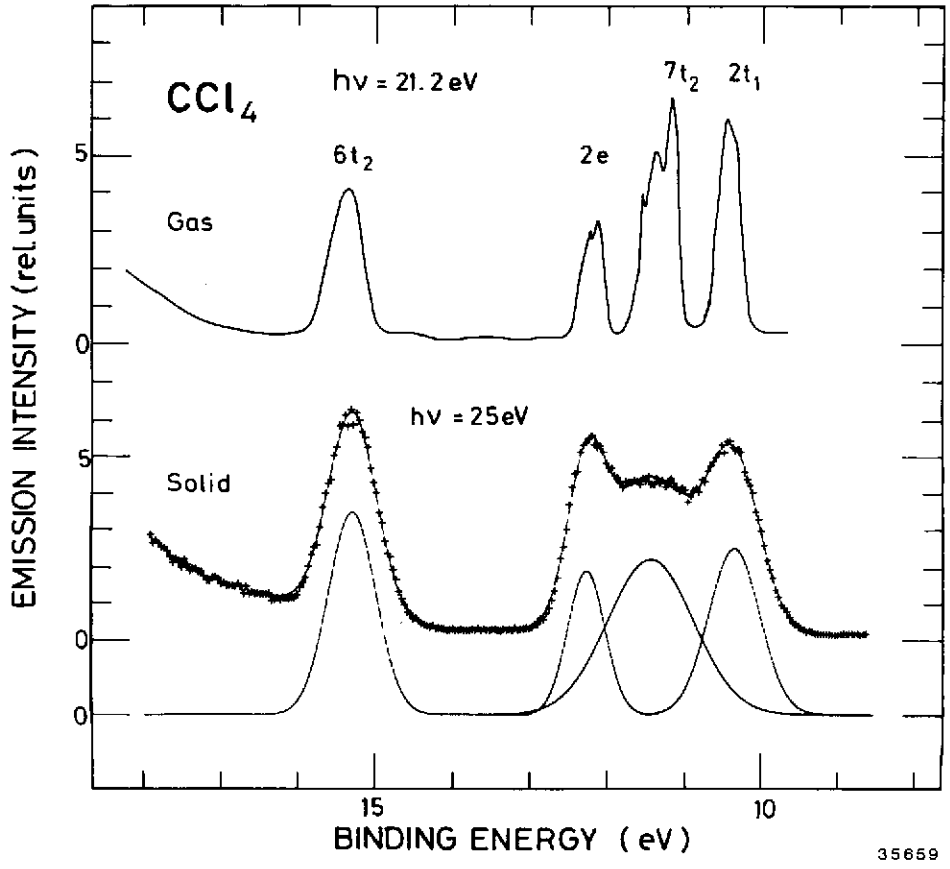
CCl_4
hν = 21.2eV
$6t_2$
2e
$7t_2$
$2t_1$
Gas
hν = 25eV
Solid
EMISSION INTENSITY (rel.units)
BINDING ENERGY (eV)
35659

Fig. 12

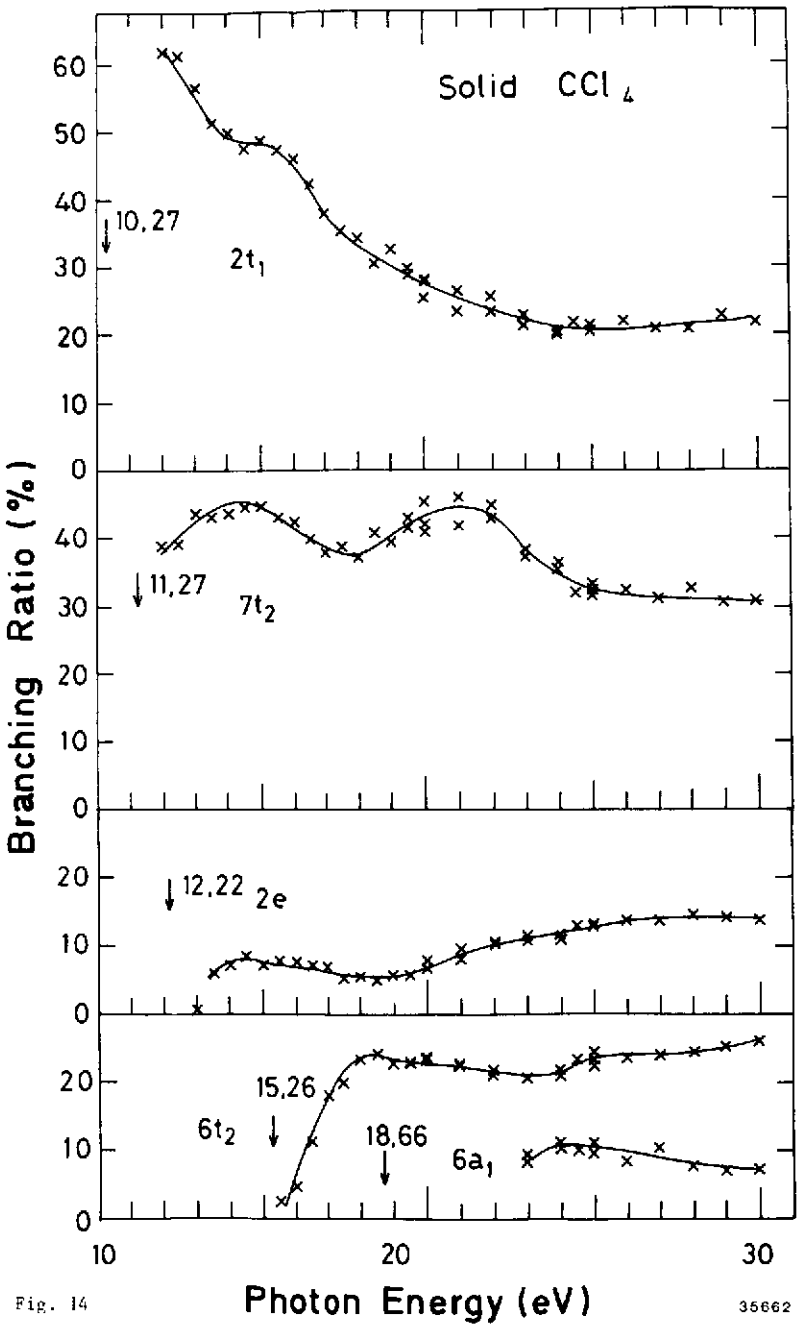
Solid CCl 4
10,27
2t1
11,27
7t2
12,22
2e
15,26
6t2
18,66
6a1
Branching Ratio (%)
Photon Energy (eV)
35662

Fig. 14